



CHORUS

This is the accepted manuscript made available via CHORUS. The article has been published as:

Photomechanical effect leading to extraordinary ductility in covalent semiconductors

Hongwei Wang, Shuangxi Song, Xinshu Zou, Fangxi Wang, Zhifu Zhang, Sergey I. Morozov, Xiaodong Wang, Kolan Madhav Reddy, and Qi An

Phys. Rev. B **100**, 094110 — Published 30 September 2019

DOI: [10.1103/PhysRevB.100.094110](https://doi.org/10.1103/PhysRevB.100.094110)

Photomechanical Effect Leading to Extraordinary Ductility in Covalent Semiconductors

Hongwei Wang^{1†}, Shuangxi Song^{2†}, Xinshu Zou², Fangxi Wang¹, Zhifu Zhang², Sergey I. Morozov³, Xiaodong Wang², Kolan Madhav Reddy^{2*}, Qi An^{1*}

¹*Department of Chemical and Materials Engineering, University of Nevada-Reno, Reno, Nevada 89557, United States.*

²*State Key Laboratory of Metal Matrix Composites, School of Materials Science and Engineering, Shanghai Jiao Tong University, Shanghai 200240, China.*

³*Department of Physics of Nanoscale Systems, South Ural State University, Chelyabinsk 454080, Russia.*

*Corresponding author-Email: qia@unr.edu, kmreddy@sjtu.edu.cn

† These authors are contributed equally to this work

Abstract

Covalent semiconductors play an important role in key technological advancements such as communications, consumer electronics, automotive, energy, and more. However, low ductility of covalent semiconductors, originating from the strong chemical bonding, prevents them from widely engineering applications. In this work, we demonstrate that the bond strength of covalent materials is very sensitive to the electron distribution, able to be effectively modified via the electron-hole pairs (EHPs) induced by photo-excitation. The photomechanical effects in III-V covalent semiconductors GaP, GaAs and InP have been examined by the combination of the advanced quantum mechanics (QM) simulations, nanoindentation experiments, and state-of-the-art transmission electron microscopy (TEM) measurements. The QM results indicate that the energy barrier for deformation slip in GaP is reduced by more than 50% by generating high concentration EHPs ($\sim 10^{21} \text{ cm}^{-3}$), exhibiting the metal-like ductility. The theoretical prediction agrees very well with the experimental measured performance where more dislocations are activated under light-illumination conditions.

PACS number(s): 61.82.Fk, 62.20.-x, 62.20.Fe, 61.72.Lk, 61.72.Mm, 62.20.Dc

I. INTRODUCTION

Manufacture of modern electronic devices desires strong and ductile inorganic semiconductors. However, the inorganic semiconductors normally exhibit poor plasticity and low ductility at the room temperature [1], due to the high energy barrier for dislocation activation caused by the strong covalent or ionic interatomic bonding [2,3]. On the other hand, dislocations are general deleterious to the electronic properties of semiconducting devices because they could generate trapping electronic states facilitating the electron-hole recombination. Therefore, it is essential to control dislocations in inorganic semiconductors for their practical applications in optical and electronic device technology [4].

The fundamental unit of carrier generation and recombination in semiconducting devices is electron-hole pair (EHP) which can be generated by photo-excitation or thermal-excitation [5,6]. In addition to determining the electronic properties, the EHP has been found to significantly influence the mechanical properties of inorganic semiconductors [5–7]. Unlike metallic systems, the chemical bonds in inorganic semiconductors strongly depend upon the electron distribution [4] and can be extensively modified by EHP carriers. As a result, the mechanical properties associated with the bond strength should be altered with the excited EHPs as well. Recent experimental work has indicated that the mechanical behavior of ionic semiconductor ZnS can be effectively controlled by light illumination [5]. The ZnS crystal displays the brittle character under light condition, however it exhibits extraordinary plasticity in complete darkness. Such phenomenon of light dependent mechanical property and related dislocation behavior are called photomechanical or photoplastic effect [8,9]. We proposed that the strength of the ionic bonds can be dramatically reduced by the light excited electron-hole pairs [7], which account for the large the photomechanical effect in ZnS.

Besides ionic semiconductors, the covalent semiconductor GaAs also exhibits the cathodoplastic effect experimentally [6]. Its mechanical deformation is enhanced by the EHPs generated via electrons from the imaging beam in nondestructive scanning electron microscopy. The photomechanical effects have been examined extensively in ionic semiconductors through a flow of charge in the direction of slip [10,11], but knowledge of these effects on the covalent semiconductors remain limited. Since the interatomic binding forces are dramatic different between ionic and covalent crystals, the excited carriers induced plasticity in covalent semiconductors is expected to be a different mechanism. Hence, the microscopic origin of the photomechanical or cathodoplastic effect in covalent semiconductors is essential to be investigated, which may provide useful guidance for developing advanced semiconductors with superior mechanical behaviors.

In this work, we have combined constrained density functional theory (CDFT) [12–18], nanoindentation, and transmission electron microscopy (TEM) to examine the photomechanical properties and underlying the mechanical deformation

mechanism in III-V covalent semiconductors. Our CDFT simulations indicate that all the covalent semiconductors mentioned in our work tend to become more ductile under light illumination. More important, our simulations elucidated the electronic origin for how the excited carriers regulate the mechanical properties in covalent semiconductors. Further nanoindentation and TEM studies verified the underlying deformation mechanism for the enhanced plasticity of GaP in a light illumination compared with complete darkness.

II. EXPERIMENTAL AND THEORETICAL METHODS

We carried out ab initio DFT calculations based on the projector augmented wave (PAW) method [18] within the framework of generalized gradient approximation [15] using the VASP package [16,17]. The planewave basis set cutoff was set as 450 eV for all cases, and a Γ -centered $6 \times 6 \times 1$ k-point mesh was used for Brillouin zone integration, which was sufficient for good convergences of total energy and forces acting on atoms. The energy and force convergence tolerances for structural relaxations are 1×10^{-6} eV and $5 \text{ meV}/\text{\AA}$, respectively. The VESTA software [19] is used to visualize crystal structures and plot charge densities. The generalized stacking fault energy (GSFE) profile is simulated with the slab model in which one half of atomic layers were rigidly shifted related to the second half by a displacement towards a specific direction on the $\{111\}$ plane. The slab model cannot be separated by vacuum layers, due to the impurity states introduced by dangle bonds on the free surface of covalent semiconductors. Therefore, the slab model was constructed with the supercell without vacuum layers, meeting the periodic boundary condition. The supercell has to consist of three slabs including three stacking fault planes, and the three slabs are relatively slipped by a same amount displacement towards three different but symmetry-equivalent $\langle 11\bar{2} \rangle$ or $\langle 1\bar{1}0 \rangle$ directions [20]. The cell parameters and atom positions were only allowed to relax perpendicular to the $\{111\}$ slip plane. In order to obtain the GSFE profile under light-irradiation, the electronic occupation matrixes are fixed to the particular electron-hole excited configurations when the structure relaxations were performed. The excited electron or hole occupation matrix is obtained through adding an electron to or removing an electron from the neutral system, respectively. The Crystal Orbital Hamilton population (COHP) analysis for chemical-bonding were performed using the LOBSTER package [21], enabling to process PAW-based output from the VASP package. The orbital charge for a specific chemical bond was calculated with the periodic Natural Bond Orbital software [22].

Single crystals GaP, with the sample size of $10 \text{ mm} \times 10 \text{ mm} \times 1 \text{ mm}$, was grown by Czochralsky method (Moltech GmbH) and was used for the mechanical

deformation tests. Then nanoindentation tests were performed under complete darkness and visible light using a Hysitron Ti-950 nanoindenter equipped with a Berkovich tip. The transmissivity of GaP is around 70% in the visible light range. The applied visible light source is 3150 K color temperature with the wavelength (λ) from 500 to 600 nm. All the nanoindentation tests were carried out on the $\langle 110 \rangle$ crystallographic orientation of GaP single crystals. The maximum applied load was 13 mN and the time to load is 10 second. The holding time is 2 second and the unloading time is 5 second, respectively. The hardness and elastic modulus of single crystal GaP in complete darkness and illumination light were obtained separately from more than 15 indentation tests. The indentation specimens are cross sectioned to a thin foil using focused ion beam (FIB) milling system (FEI Versa3D) for TEM characterization. Prior to TEM observations, the FIB cross-sectioned both under darkness and illuminated light thin foils were gently milled by the Fishone 1040 Nanomill system at 500 eV for 15 mins to remove Ga⁺ contamination without altering the chemistry and structure of specimens. The microstructures of undeformed and deformed GaP specimens were characterized using JEM-ARM 200 F atomic resolution analytical microscope equipped with imaging Cs corrector and probe forming Cs corrector were used separately to acquire atomic resolution images and dislocation structures.

III. RESULTS AND DISCUSSION

The III-V semiconductors GaP, GaAs, and InP, have the same sphalerite crystal structure, belonging to $F\bar{4}3m$ space group [23,24]. The deformation slip in these semiconductors prefers to occur along the $\{111\}$ plane. The most common complete dislocation generated by the deformation slip is along the $\langle 1\bar{1}0 \rangle$ direction [10,25] with the smallest Burgers vector $\vec{b} = 1/2\langle 1\bar{1}0 \rangle$. However, the $\{111\}\langle 1\bar{1}0 \rangle$ dislocation is prone to dissociate into two Shockley partial dislocations [26,27] with Burgers vectors $1/6\langle 2\bar{1}\bar{1} \rangle$ and $1/6\langle 1\bar{2}1 \rangle$ (symmetry equivalent with the $1/6\langle 11\bar{2} \rangle$) to lower the misfit energy. Hence, only the $\{111\}\langle 1\bar{1}0 \rangle$ and $\{111\}\langle 11\bar{2} \rangle$ slip systems are considered in the present work. Moreover, the $\{111\}\langle 1\bar{1}0 \rangle$ slip system can be activated through either the widely spaced planes or narrowly spaced ones, denoted as path I and path II, respectively (see Fig. 1).

The deformation slip can be theoretically investigated by calculating the GSFE profile, known as γ -surface [26,28] from which one can derive the important information such as the Peierls barrier [29] as well as stacking fault (SF) energy. Figs. 1(a)-1(c), display the DFT predicted GSFE curves of GaP, as a function of lattice displacement $u/|\vec{b}|$, where u represents the magnitude of displacement. The energy curves marked with the $0h^+0e^-$, $1h^+1e^-$, and $2h^+2e^-$ represent the γ -surface at ground state, excited state with one EHP, and excited state with two EHPs,

respectively. The crystal structure of GaP and its two plausible deformation slip pathways along the widely stacked Ga and P atomic (Ga-P) layers (path I), or along the closely stacked Ga-P layers (path II) are displayed in Fig. 1(d). As shown in Fig. 1(a), along GSFE curves of the $\langle 11\bar{2} \rangle$ slip (path I) there are two saddle points and one valley point, which are named as the unstable stacking fault (USF) energy, γ_{us} , the unstable twin fault (UST) energy, γ_{ut} , and the intrinsic stacking fault (ISF) energy, γ_{isf} , respectively. The atomic structures of the USF for path I are shown in Fig. 1(e), in which the Ga-P covalent bonds are broken along the slip plane, resulting in significantly increased energy barriers for the deformation slip. In the UST structure shown in Fig. 1(f), the same kind of atoms between the spaced layers are completely opposite to each other along the slip plane, accounting for the maximum energy barrier on the GSFE curves.

As shown in Fig. 1(b), the maximum energy barrier for the $\{111\}\langle 1\bar{1}0 \rangle$ deformation slip is higher than the γ_{us} of the $\{111\}\langle 11\bar{2} \rangle$ slip system, indicating that the perfect dislocation slip with the Burgers vector $1/2\langle 1\bar{1}0 \rangle$ is energy favorable to split into two $1/6\langle 11\bar{2} \rangle$ partial dislocations. The GSFE curves of the $\{111\}\langle 11\bar{2} \rangle$ slip system on path II are plotted in Fig. 1(c), and the relevant USF and UST structures are shown in Fig. 1(g) and 1(h). The seriously shortened Ga-P distances in the UST structure lead to an extremely high γ_{ut} for path II. Therefore, only GSFE curves for the partial $\{111\}\langle 11\bar{2} \rangle$ slip are shown in Fig. 1(c). The GSFE curves of the complete dislocation-displacement vector $1/2\langle 11\bar{2} \rangle$ are displayed in Fig. S1(a) of the Supplemental Material (SM) [30]. The $\{111\}\langle 1\bar{1}0 \rangle$ deformation slip on path II can also result in the seriously shortened Ga-P bonds as well as extremely high energy barriers, as shown in Fig. S1(d) of the SM [30].

It is evident to be found in Figs. 1(a)-1(c), the entire GSFE profiles are dramatically decreased by the photoexcitation induced EHPs. In particular, the energy barrier for the $\{111\}\langle 11\bar{2} \rangle$ deformation slip on the path I is reduced by sixty percent via two excited EHPs, corresponding to a carrier concentration of $\sim 10^{21} \text{ cm}^{-3}$. As shown in Figs. 1(a)-1(c), the path II is energy favorable to develop deformation slip at the ground state, which is well consist with the previous theoretical and experiment investigations [10]. As the concentration of EHPs increases, the γ_{us} of path I is gradually dropped below that of path II, indicating path I show an increased tendency to generate deformation slip under strong light illumination condition.

The above analysis indicate that the photoexcitation has a significant impact on the GSFE profile for the deformation slip, leading to modulated mechanical behaviors. The primary mechanisms for plastic deformation in face-centered cubic crystals at low temperature are developed through dislocation slip and deformation twinning [31,32]. It has been well known that when the dislocation slip is the main deformation mode, the materials tend to exhibit a ductile character. However, the twin

boundary is likely to block the dislocation motion similar to the conventional grain boundary, making the materials undergo the small mechanical strain and display a more brittle character [33]. To describe tendency for microtwin formation relative to dislocation nucleation, we examined the twinnability of GaP which is dependent on the ratios of $\gamma_{\text{isf}}/\gamma_{\text{us}}$ and $\gamma_{\text{us}}/\gamma_{\text{ut}}$ [31,32]. The details can be find in the SM [30]. A summary of the number for γ_{us} , γ_{ut} , and twinnability τ of path I are given in Table SI of the SM [30]. The twinnability of GaP decreases as the photoexcitation enhances, suggesting that GaP is prone to generate more dislocation slip through the path I under light condition, due to the significantly decreased γ_{us} as well as the reduced twinnability. In addition, the twinnability for path II remains very small even with the decreased γ_{us} and γ_{ut} with the photoexcitation, suggesting the major dislocation mechanism under illumination. Hence, the GaP semiconductor is expected to become more ductile with light exposure.

To illustrate the microscopic mechanism for the large photomechanical effect in these III-V covalent semiconductors, we performed charge density and chemical bonding analyses associated with the deformation slip. The results of the electron localization function (ELF) [34] and bonding charge density shown in Fig. S2 of the SM [30] indicate that the electrons prefer to localize around the bonding center in GaP, GaAs, and InP semiconductors, showing an ideal covalent bonding character. Therefore, we utilize a quantum mechanical bonding indicator COHP [35,36] to analyze the chemical bond, which can capture the subtle change of bonding nature in covalent systems during the deformation slip. Figs. 2(a)-2(c), display the COHP analysis, the charge distribution of conduction band minimum (CBM) and valence band maximum (VBM) of GaP at the ground state. The charge transfer processes of the photoexcitation for the perfect structure, USF structure, and UST structure are also included in the bottom part of Fig. 2. The valence and conduction bands are composed of the Ga-P bonding and antibonding states in the perfect GaP structure [see Fig. 2(a)]. The charge densities contributed from VBM (blue) and CBM (yellow) exhibit the bonding and antibonding characters, well consistent with the COHP analysis. When the photoexcitation occurs, the electrons will transfer from the bonding states to the antibonding states, creating the electron and hole pairs marked with violet and green isosurfaces. This electron transfer weakens the bonding strength to lower the energy barrier for the deformation slip.

The CBM electronic state for the USF structure of path I is shown in Fig. 2(b), exhibiting a weaker Ga-P bonding character different from that of the undeformed structure. This CBM bonding state mainly distributes around the Ga atom on the slip plane, similar to the shape of the electron isosurface in the density diagram of the excited EHP. The Fermi level also touches the bonding state in the COHP analysis, showing an agreement with the charge density results [see Fig. 2(b)]. After the electrons are excited from VBM to CBM, these bonding CBM electronic states will rebuild new weak chemical bonds with a strength of 20% Ga-P perfect bond on the slip plane. The deformation slip can be further promoted because of these new created

chemical bonds with a bond length of 3.15 Å. As for the UST structure of path I [see Fig. 2(c)], the CBM electronic state also becomes the Ga-P bonding state but weaker than that in the USF structure, due to the longer Ga-P distance of 3.36 Å. This accounts for the reduction of the γ_{ut} less than that of the γ_{us} as well as the decreased twinnability for deformation slip on the path I, under the light illumination condition. The mechanism for photoexcitation reduced energy barrier of the deformation slip on path II is also attributed to the reformed chemical bonds on the slip plane. More details can be found in Fig. S3(a) of the SM [30].

On the basis of the same theoretical framework with the GaP system, we investigated GaAs and InP semiconductors, which also exhibit the large photomechanical effect and become more ductile under illumination condition. The GSFE curves, bonding and charge analysis for the deformation slip in GaAs and InP systems are shown in Figs. S1-S5 of the SM [30]. Their GSFE profiles undergo an evident reduction and show a decreased tendency for twinnability as the photoexcitation carriers increase. The photoexcitation results in the GaP-like bonding breaking and reforming processes in GaAs and InP, which account for the significant ductility improvement.

To determine the intrinsic deformation mechanism and how this is affected by EHPs, we applied finite shear deformation on GaP along the most plausible slip system $\{111\}\langle 11\bar{2}\rangle$ under $0h^+0e^-$ and $1h^+1e^-$ states. The energy and the shear stress of GaP as a function of the shear strain are shown in Fig. 3(a), where the shear strain is given as $(u/|\vec{b}|)100\%$, and u is the displacement of the end point of lattice vector \vec{c} along the Burgers vector \vec{b} . The elastic energy and shear stress for the $1h^+1e^-$ state are significantly decreased in contrast to those for the $0h^+0e^-$ state at the same shear strain. The explanation for the reduced shear stress is due to antibonding and bonding characters of the CBM and VBM electronic states (The plotted charge distribution for sheared GaP structure at the elastic limit are shown in Fig. S6.). The photoexcitation EHPs weaken the bonding strength to reduce the shear stress and shear energy. The results show a good agreement with the conclusion from GSFE results. Finally, we applied the empirical Pugh's criterion [37], the ratio of shear modulus G over bulk modulus B , to measure the brittleness/ductility quantity [1,37,38]. The G/B predictor indicates that the GaP crystal exhibits the extraordinary ductility close to some metallic materials such as Fe and Ni. More details are discussed in the supplementary text.

In order to validate the theoretical predication and underly the deformation mechanism associated with darkness and brightness conditions, we performed nanoindentation experiments and TEM on the sphalerite GaP. The large-size single crystal GaP specimens with an optical transmittance of 70% were used for the

deformation tests as shown in [(Fig. S7(a)]. Annular dark field scanning transmission electron microscopy (ADF-STEM) image acquired from the as-received GaP shows nearly perfect structure and atomic position of Ga (red color) and P (green color) atoms visualized along $\langle 110 \rangle$ zone axis [Fig. S7(b)]. The deformation tests on GaP single crystals were performed separately by nanoindentation in a complete darkness and light conditions [Figs. S8(a) and S8(b)]. Fig. S9 shows representative loading-unloading curves of indentation performed in a darkness and brightness at an identical loading condition (details in the SM). The brightness GaP indent curve in Fig. S9 undergoes a larger penetration depth during loading and a steep slope during unloading as compared to darkness GaP crystal. The measured hardness (H) and elastic modulus (E) values of darkness GaP [Figs. 3(b) and 3(c)], were about 11.63 ± 0.12 GPa and 166 ± 1.65 GPa, whereas H and E values of brightness GaP were only of 10.80 ± 0.32 GPa and 135.97 ± 6.07 GPa. The estimated H and E values of brightness GaP are reduced considerably by $\sim 8\%$ and 20% as compare to darkness GaP, indicating that the GaP is softened under light illumination. In addition, brightness GaP loading curve shows the significant displacement bursts, or pop-ins denoted by black arrowheads (Inset Fig. S9). The pop-ins are often associated with elastic-to-plastic transition, which triggered by dislocations nucleation suggesting that extensive plastic deformation could take place under the light-illumination condition [38]. The reduced elastic modulus, which is proportional to the bulk modulus and shear modulus, is consistent with our theoretical predictions [Fig. 3(a)].

Fig. 4 shows TEM micrographs of indented GaP specimens under complete darkness and light-illumination conditions, respectively. Fig. S10 of the SM [30] displays the typical cross sectioned indentation specimen lifted-out using focused ion beam (FIB) milling for TEM observations. A representative bright field TEM (BF-TEM) image beneath the indentation region performed in the darkness condition [Fig. 4(a)] shows the induced stress as appears in dark contrast are parallel to the $\langle 110 \rangle$ loading direction. Fig. 4(b) shows diffraction contrast TEM image obtained from the same region in Fig. 4(a) revealing several planar defects that were visible as a thin line when imaged on the $\{111\}$ planes, suggesting that the displacement vector is parallel to $\langle 110 \rangle$ zone axis. These defects can be recognized as the stack fault in the high resolution TEM (HRTEM) image to be parallel to onset of the $(11\bar{1})$ plane as shown in Fig. 4(c). Inset calculated image of GaP oriented along the $[10\bar{1}]$ zone axis shows the experimentally observed undeformed atomic structure in which atomic position of Ga (red dots) and P (green dots) can be directly visualized.

In contrast, the deformation behavior dramatically changes in the light condition (Fig. S11 of the SM [30]) when the sample experiences a constant loading force of Fig. 4(a). A typical BF-TEM image beneath the indent shows that the large deformation area induced by high stresses is dominated by dislocation slip lines that are mostly parallel to the $\langle 110 \rangle$ direction [(Fig. 4(d)]. The diffraction contrast TEM image shows numerous dislocations of which few appears as long straight dislocation lines and other dislocations had kinks indicated by red arrowhead in Fig. 4(e) and Fig.

S11. We did not observe any dislocation entanglements or evidence of cross slip. The observed HRTEM image [Fig. 4(f)] reveals a straight dislocation slip line is moving along the $(11\bar{1})[101]$ slip system. Although the high densities of dislocations are detected under illumination conditions, their individual dislocation core cannot be imaged using HRTEM due to the induced high stresses caused by nanoindentation. The image of Fig. 4(f) demonstrates that slip band with a width of ~ 1.5 nm are formed with 5 to 6 atomic spacing to be constrained on the specific plane appears to be mixed dislocations [39].

IV. CONCLUSIONS

In summary, the photomechanical effects on III-V semiconductors GaP, GaAs, and InP were investigated by the combination of CDFT simulations, nanoindentation, and TEM experiments. Our results indicated that the III-V semiconductors become more ductile under light irradiation. The microscopic origin for this large photomechanical effect is attribute to the modified bonding nature by excited EHPs. This can cause the reduced energy barrier for the deformation slip and make the covalent crystals more ductile under light-illumination. In contrast, the modified energy barrier for the deformation slip results from weakened coulomb force by the photoexcitation carriers in ionic crystals [7]. Another factor for this light induced ductile behavior in III-V semiconductors is the electron deficient character of sp^3 hybridization bonds. Taking GaP crystal as an example, each Ga or P provides three electrons to form four sp^3 hybridization bonds. The bonding charge for each Ga-P bond is $1.33e$, which are obtained from the natural bond orbital analysis [22]. The six shared electrons make these four sp^3 bonding orbitals partially occupied, resulting in the Ga-P bonds with the weak strength easier to be tailored.

Acknowledgements

We would like to thank Professor Guo Qiang (Shanghai Jiao Tong University) for the allowing using Nanomill instrument. SM was thankful for the support by Act 211 Government of the Russian Federation, under No. 02.A03.21.0011 and by the Supercomputer Simulation Laboratory of South Ural State University. This work was supported by the National Science Foundation (CMMI-1727428) and National Natural Science Foundation of China (Grant No. 51850410501).

Competing Interests: The authors declare that they have no competing financial interests.

References

- [1] S. Ogata, J. Li, N. Hirotsuki, Y. Shibutani, and S. Yip, Phys. Rev. B **70**,104104 (2004).
- [2] Y. Zhang, H. Sun, and C. Chen, Phys. Rev. Lett. **94**, 145505 (2005).
- [3] R. Whitworth, Adv. Phys. **24**, 203 (1975).
- [4] M. Cardona and Y. Y. Peter, *Fundamentals of Semiconductors* (Springer, 2005).
- [5] Y. Oshima, A. Nakamura, and K. Matsunaga, Science **360**, 772 (2018).
- [6] P. G. Callahan, B. B. Haidet, D. Jung, G. G. Seward, and K. Mukherjee, Phys. Rev. Mater. **2**,

- 081601 (2018).
- [7] H. Wang, S. I. Morozov, W. A. Goddard III, and Q. An, *Phys. Rev. B* **99**, 161202 (2019).
 - [8] L. Carlsson and C. Svensson, *J. Appl. Phys.* **41**, 1652 (1970).
 - [9] L. Carlsson and C. Ahlquist, *J. Appl. Phys.* **43**, 2529 (1972).
 - [10] V. F. Petrenko and R. W. Whitworth, *Philos. Mag. A* **41**, 681 (1980).
 - [11] C. C. Speake, P. J. Smith, T. R. Lomer, and R. W. Whitworth, *Philos. Mag. A* **38**, 603 (1978).
 - [12] B. Kaduk, T. Kowalczyk, and T. Van Voorhis, *Chem. Rev.* **112**, 321 (2012).
 - [13] M. Melander, E. Ö. Jónsson, J. J. Mortensen, T. Vegge, and J. M. García Lastra, *J. Chem. Theory Comput.* **12**, 5367 (2016).
 - [14] D. Kidd, A. S. Umar, and K. Varga, *Phys. Rev. B* **98**, 075108 (2018).
 - [15] J. P. Perdew, K. Burke, and M. Ernzerhof, *Phys Rev Lett* **77**, 3865 (1996).
 - [16] G. Kresse and J. Hafner, *Phys. Rev. B* **47**, 558 (1993).
 - [17] G. Kresse and D. Joubert, *Phys Rev B* **59**, 1758 (1999).
 - [18] P. E. Blöchl, *Phys. Rev. B* **50**, 17953 (1994).
 - [19] K. Momma and F. Izumi, *J. Appl. Crystallogr.* **44**, 1272 (2011).
 - [20] A. Nakamura, M. Ukita, N. Shimoda, Y. Furushima, K. Toyoura, and K. Matsunaga, *Philos. Mag.* **97**, 1281 (2017).
 - [21] S. Maintz, V. L. Deringer, A. L. Tchougréeff, and R. Dronskowski, *J. Comput. Chem.* **37**, 1030 (2016).
 - [22] B. D. Dunnington and J. R. Schmidt, *J. Chem. Theory Comput.* **8**, 1902 (2012).
 - [23] K. Morizane, *J. Cryst. Growth* **38**, 249 (1977).
 - [24] D. N. Talwar and B. K. Agrawal, *Phys. Status Solidi B* **63**, 441 (1974).
 - [25] C. Levade and G. Vanderschaeve, *J. Cryst. Growth* **197**, 565 (1999).
 - [26] M. Jahnátek, J. Hafner, and M. Krajčí, *Phys. Rev. B* **79**, 224103 (2009).
 - [27] D. Hull and D. J. Bacon, *Introduction to Dislocations*, 4th ed (Butterworth-Heinemann, Oxford [Oxfordshire] ; Boston, 2001).
 - [28] Z. Pei, L.-F. Zhu, M. Friák, S. Sandlöbes, J. von Pezold, H. W. Sheng, C. P. Race, S. Zaeferrer, B. Svendsen, D. Raabe, and J. Neugebauer, *New J. Phys.* **15**, 043020 (2013).
 - [29] G. Lu, N. Kioussis, V. V. Bulatov, and E. Kaxiras, *Phys. Rev. B* **62**, 3099 (2000).
 - [30] See Supplemental Material at [URL will be inserted by publisher] for supplementary text of twinnability analysis, theoretical investigations for the mechanical behaviors of GaAs and InP, analysis of Pugh's criterion, and Image simulation; Table S1 of computed unstable-stacking energy, unstable-twinning energy, and approximate twinnability for sphalerite covalent crystals; and Supplementary figures (S1-S11) including: (i) GSF energy landscapes of sphalerite covalent crystals, (ii) electronic structure analysis for deformation slip in sphalerite covalent crystals, (iii) GaP specimen and ADF-STEM image, (iv) nanoindentation load-depth curves, (v) cross-sectional TEM sample preparation by FIB milling, and (vi) TEM image of GaP deformed under illumination light.
 - [31] E. B. Tadmor and S. Hai, *J. Mech. Phys. Solids* **51**, 765 (2003).
 - [32] E. B. Tadmor and N. Bernstein, *J. Mech. Phys. Solids* **52**, 2507 (2004).
 - [33] Y. T. Zhu, X. Z. Liao, and X. L. Wu, *Prog. Mater. Sci.* **57**, 1 (2012).
 - [34] A. Savin, R. Nesper, S. Wengert, and T. F. Fässler, *Angew. Chem. Int. Ed. Engl.* **36**, 1808 (1997).
 - [35] R. Dronskowski and P. E. Bloechl, *J. Phys. Chem.* **97**, 8617 (1993).

- [36] V. L. Deringer, A. L. Tchougréeff, and R. Dronskowski, *J. Phys. Chem. A* **115**, 5461 (2011).
 [37] S. F. Pugh, *Lond. Edinb. Dublin Philos. Mag. J. Sci.* **45**, 823 (1954).
 [38] D. Roundy, C. R. Krenn, M. L. Cohen, and J. W. Morris, *Phys. Rev. Lett.* **82**, 2713 (1999).
 [39] J. V. Barth, H. Brune, G. Ertl, and R. J. Behm, *Phys. Rev. B* **42**, 9307 (1990).

Figures

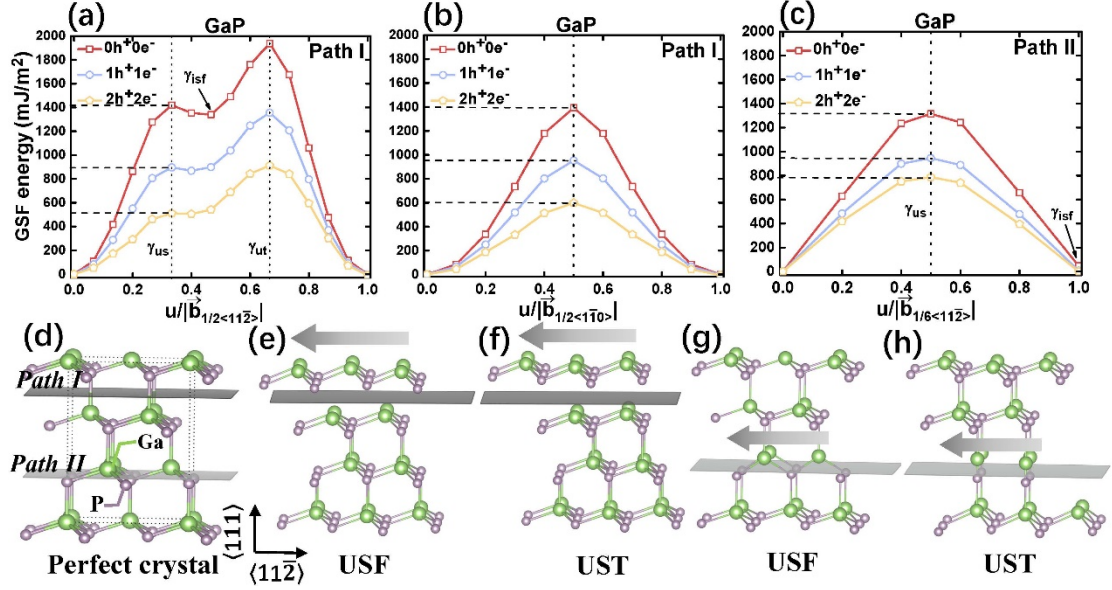


FIG. 1. (a), (b) The variation of GSF energy with the displacement $u/|\vec{b}|$ along the $\langle 11\bar{2} \rangle$ (a) and $\langle 1\bar{1}0 \rangle$ (b) directions on the path I, where \vec{b} is the length of the Burgers vector and u represents the magnitude of displacement. The GSF energy curves for ground state ($0h^+0e^-$), one electron-hole excited ($1h^+1e^-$) state, and two electron-hole excited ($2h^+2e^-$) state, respectively. The notations γ_{us} , γ_{isf} and γ_{ut} represent the USF energy, ISF energy, and UST energy, respectively. (c) GSF energy as a function of the displacement $u/|\vec{b}|$ along the $\langle 11\bar{2} \rangle$ direction on the path II. (d) A schematic showing two possible plastic deformation slip paths along the $\{111\}$ planes. (e), (f) Illustration of the USF (e) and UST (f) structures along path I. (g), (h) Illustration of the USF (g) and UST (h) structures along path II. Ga and P atoms are represented by green and violet balls, respectively.

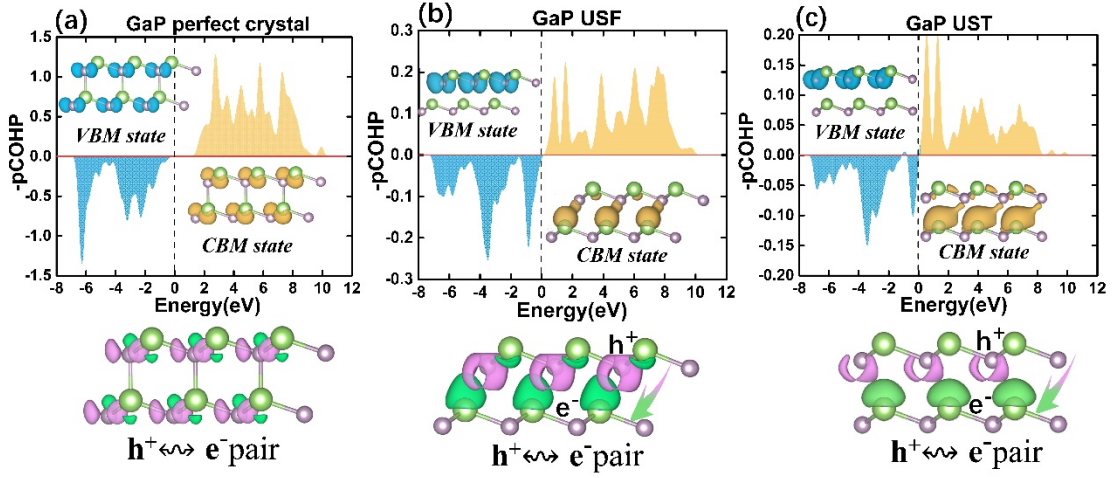


FIG. 2. COHP analysis for the bond interactions in the undeformed (a), USF (b), and UST (c) structures; and the electronic orbitals of the conduction band minimum (CBM, blue) and valence band maximum (VBM, yellow); and the hole (violet) and electronic (green) densities induced by photo-excitation shown on the bottom.

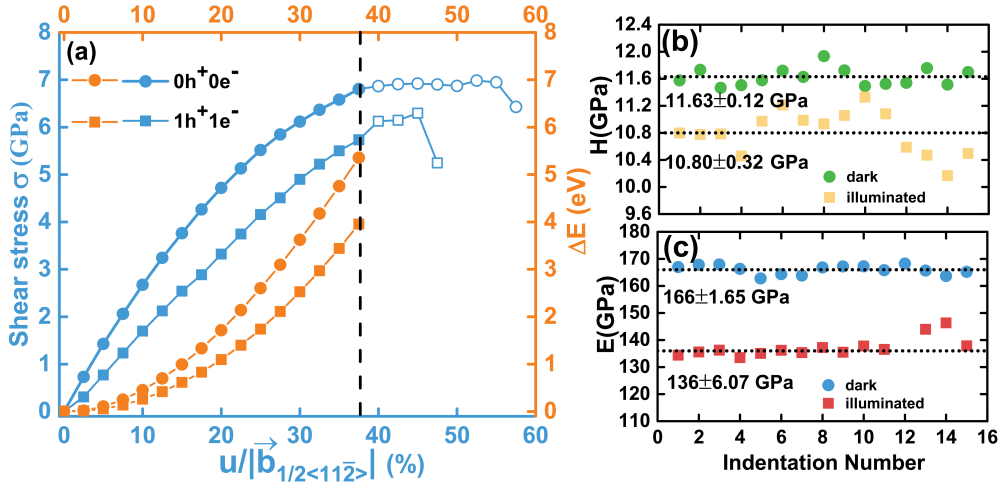


FIG. 3. The theoretical and experimental investigations for the mechanical properties of GaP. (a) The dependences of shear stress (blue color) and energy (yellow color) on the $\{111\}\langle 11\bar{2}\rangle$ shear deformation in sphalerite GaP. The circle and square symbols represent the results of the ground state and one electron-hole pair excited state, respectively. The labels ε_e and σ_e mark the strain and stress at the elastic limit. (b) Hardness and (c) elastic modulus measurements of single crystal GaP in complete darkness and light-illumination obtained from more than 15 indentation tests.

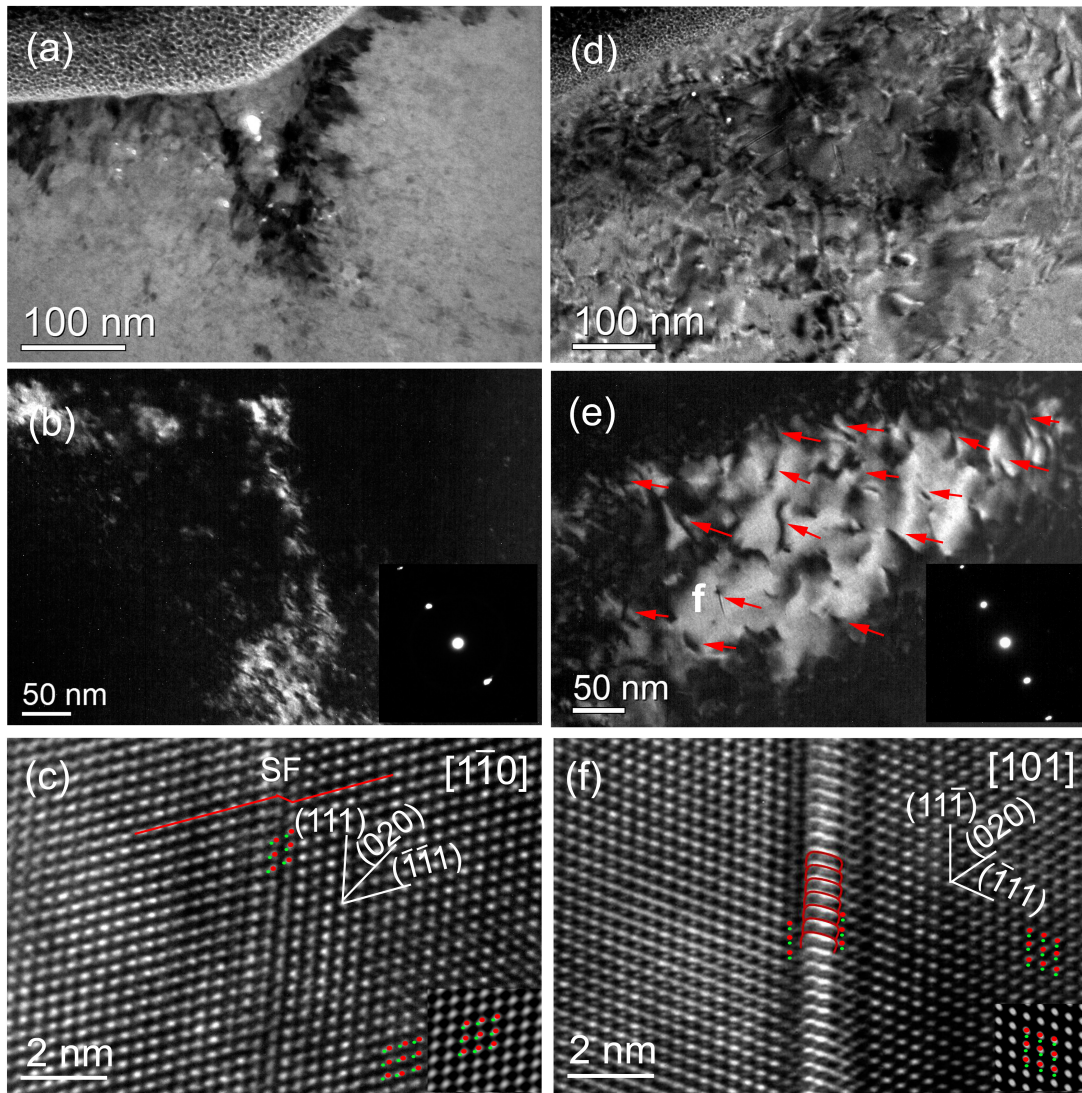


FIG. 4. (a) BF-TEM image beneath the indent region shows induced stresses in dark contrast performed under darkness. (b) Diffraction contrast TEM image, taken from the same region in (a), displays several thin straight faults along $\{111\}$ planes. (c) Atomic resolution TEM image reveals that the thin straight defects are stacking faults parallel to (111) plane. (d) A representative BF-TEM image shows higher deformability beneath the indent region performed under light illumination. (e) Dark contrast TEM, acquired from the same region in (d), displays the large number of straight and bending dislocations slip occur along $\{111\}$ planes. (f) HRTEM image recorded from the straight dislocation slip with width of ~ 1.5 nm marked in (e). Inset calculated image shows the consistency with undeformed atomic structure of GaP.